

RESEARCH ARTICLE

10.1029/2018JC014333

Key Points:

- Interannual modulation of EKE in the ARC region is mediated by westward propagating SSH anomalies generated by basin-wide wind stress forcing
- Upstream Agulhas Current inflow variability regulates the downstream interannual EKE fluctuations in the ARC region
- Barotropic instability is the main energy source controlling the regional EKE variability

Correspondence to:

B. Qiu,
bo@soest.hawaii.edu

Citation:

Zhu, Y., Qiu, B., Lin, X., & Wang, F. (2018). Interannual eddy kinetic energy modulations in the Agulhas Return Current. *Journal of Geophysical Research: Oceans*, 123, 6449–6462. <https://doi.org/10.1029/2018JC014333>

Received 4 JUL 2018

Accepted 13 AUG 2018

Accepted article online 23 AUG 2018

Published online 12 SEP 2018

Interannual Eddy Kinetic Energy Modulations in the Agulhas Return Current

Yanan Zhu^{1,2,3}, Bo Qiu³, Xiaopei Lin^{1,2}, and Fan Wang^{2,4}

¹Physical Oceanography Laboratory/CIMST, Ocean University of China, Qingdao, China, ²Qingdao National Laboratory for Marine Science and Technology, Qingdao, China, ³Department of Oceanography, University of Hawai'i at Mānoa, Honolulu, HI, USA, ⁴CAS Key Laboratory of Ocean Circulation and Waves, Institute of Oceanology, Chinese Academy of Sciences, Qingdao, China

Abstract Interannual variability in the mesoscale eddy field in the Agulhas Return Current (ARC) of 32–42°S and 15–35°E is investigated based on satellite altimeter observations and state estimate from the Estimating the Circulation and Climate of the Ocean, Phase II from 1993 to 2016. It is found that the interannual modulation of eddy kinetic energy in the ARC region is externally mediated by the wind stress forcing that generates the westward propagating sea surface height anomalies across the South Indian Ocean subtropical gyre. The wind-forced sea surface height anomalies influence the upstream Agulhas Current volume transports. By modulating the intensity of barotropic instability of the ARC mean flow centered around the retroflection region, the Agulhas Current inflow variability leads to the downstream interannual eddy kinetic energy fluctuations in the ARC region.

Plain Language Summary The interannual eddy kinetic energy modulations in the Agulhas Return Current region are investigated in this study on the basis of the satellite altimeter observations and the Estimating the Circulation and Climate of the Ocean, Phase II state estimate for the period of 1993–2016. The interannual eddy kinetic energy modulations in the Agulhas Return Current region are affected by the upstream Agulhas Current volume transports mainly via the barotropic instability. The wind stress curl forcing in the subtropical Indian Ocean is regarded as the major factor to modulate the Agulhas Current volume transport.

1. Introduction

The Agulhas Current system plays a critical role in interocean exchange between the Indian Ocean and Atlantic Ocean and the global climate system and has been studied extensively during the past decades (Arruda et al., 2014; Beal et al., 2011; Elipot & Beal, 2018; Leber et al., 2017; Lutjeharms, 2006; among others). Being a warm western boundary current in the Southern Indian Ocean subtropical gyre, the Agulhas Current is primarily driven by the large-scale wind stress curl between the Southern Hemisphere westerlies and southeast trade winds (Lutjeharms, 2006). It flows southwestward along the east coast of South Africa as a narrow, fast boundary current between about 27°S and 37°S and breaks until it reaches the southern tip of the African continent. It then separates and loops anticlockwise, and a significant portion of it feeds into the Southern Indian Ocean as the eastward-flowing Agulhas Return Current (ARC). Having a width of 60–80 km, the ARC shows up as a strong barotropic meander and can reach as far east as about 76°E (Arhan et al., 2003; Lutjeharms & Anson, 2001). The tight loop, known as the Agulhas retroflection (Gordon, 2003), occurs in general between 15°E and 20°E (Lutjeharms & van Ballegooyen, 1988) and has been observed to shed rings, eddies, and filaments of Agulhas Current-origin waters westward into the South Atlantic down to the depth of more than 2,000 m (Boebel et al., 2003; Gordon et al., 1992; Van Aken et al., 2003). Estimate of this eddy-mediated *Agulhas leakage* is highly uncertain, with about four to six Agulhas Rings shed from the retroflection region annually (de Ruijter, Biastoch, et al., 1999; Dencausse et al., 2010), impacting on the stability, strength, and variability of Atlantic Meridional Overturning Circulation (Biastoch et al., 2008; Weijer et al., 2002). Waters in the Agulhas Current originate mainly in the recirculating subtropical gyre of the South Indian Ocean but are also fed from the Indonesian Throughflow with relatively fresh water, from Red and Arabian Seas with salty water, and from the equatorial Indian Ocean via the East Madagascar Current and Mozambique Channel eddies (Beal et al., 2006; Z. Chen, Wu, et al., 2014; Song et al., 2004).

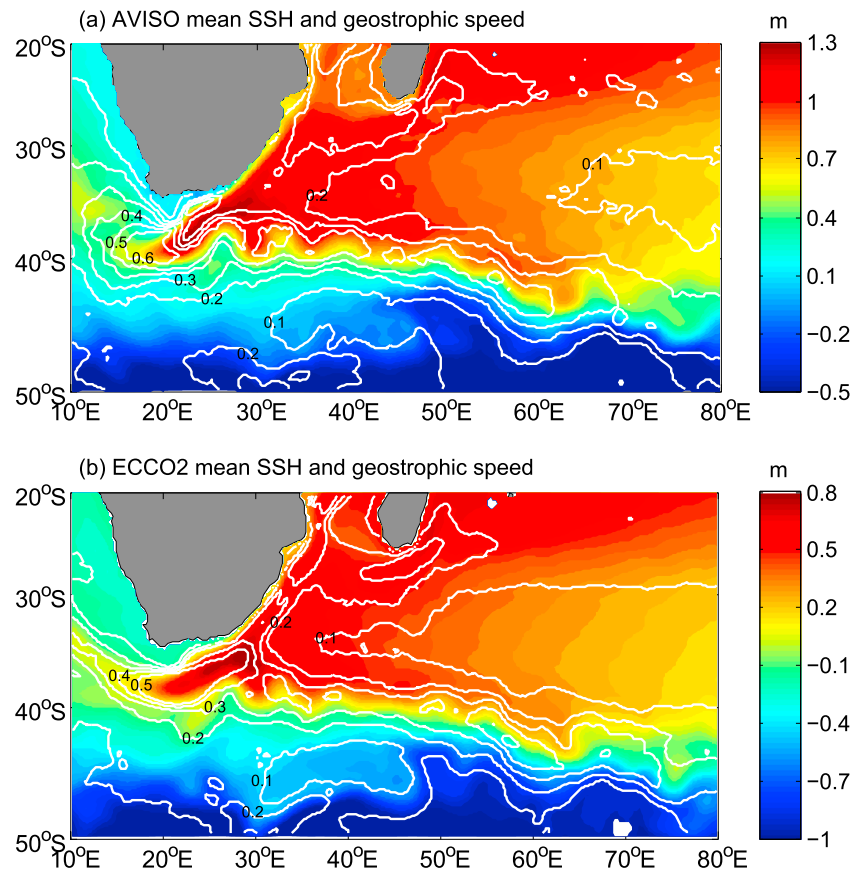


Figure 1. Mean SSH (color) and geostrophic speed (white line) distributions derived from (a) AVISO and (b) ECCO2 data during 1993–2016. SSH = sea surface height; AVISO = Archiving, Validation, and Interpolation of Satellite Oceanographic; ECCO2 = Estimating the Circulation and Climate of the Ocean, Phase II.

The Agulhas retroflection region has the highest mesoscale eddy variability in the entire Southern Ocean (Lutjeharms & van Ballegooyen, 1988). This occurs due to the fact that the longitudinal slant of the African continental slope is westward, which forces the Agulhas Current to separate at a more southwestward location than if there were no slanting African continent. Accumulation of low potential vorticity along its long path makes the Agulhas retroflection more unstable in order for it to rejoin the interior Sverdrup gyre governed by the large-scale wind stress curl. Recent studies on the Agulhas retroflection variability have mostly focused on the ring-shedding processes, showing that the increase in the Agulhas leakage activity is a response to changes of the wind forcing across the Southern Indian Ocean (Biaostoch et al., 2009). Dynamically, the ring-shedding process has been demonstrated to be related to barotropic instability of the South Indian/Atlantic supergyre (Chassignet & Boudra, 1988; Dijkstra & de Ruijter, 2001; Weijer et al., 2013).

The ARC emerges from the Agulhas retroflection and is associated with an enhanced temperature front that separates the subtropical warm water from the subpolar cold water. Belkin and Gordon (1996) detect that along the ARC path, there exist two remarkably stable meander troughs near 26°E and 35°E with a crest in between. The location of 26°E coincides with the position of the Agulhas Plateau, a major bathymetric obstacle with a 400-km-wide meridional extent (Speich et al., 2007). Dencausse et al. (2010) found that the position of the Agulhas retroflection has not varied greatly likely due to the constraint of the Agulhas Plateau based on the 20-year satellite altimetry record.

The eddy kinetic energy (EKE) reflects an important aspect of the mesoscale ocean dynamics, and its low-frequency variability has been investigated in many eddy energetic regions of the world ocean. In particular, the time-varying wind forcing has often been identified as the leading factor causing the observed low-

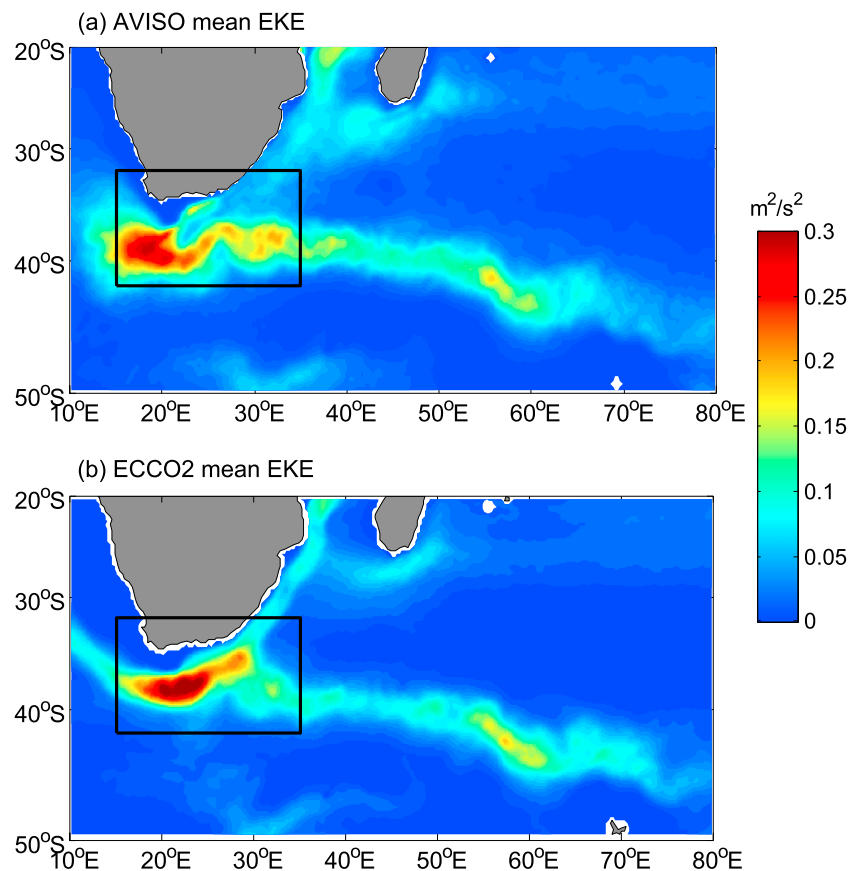


Figure 2. Mean surface eddy kinetic energy (EKE) distribution calculated from (a) AVISO and (b) ECCO2 data during 1993–2016. AVISO = Archiving, Validation, and Interpolation of Satellite Oceanographic; ECCO2 = Estimating the Circulation and Climate of the Ocean, Phase II.

frequency EKE variability (e.g., Jia et al., 2011; Qiu & Chen, 2010; Volkov & Fu, 2011). In terms of the interannual mesoscale eddy variability in the Agulhas Current system, previous studies have mostly concentrated on the upstream Mozambique Channel and the regions surrounding the Madagascar (de Ruijter et al., 2004; Palastanga et al., 2006; Schouten et al., 2003). They found that the interannual fluctuations of EKE associated with the sea surface height (SSH) variations inside the Mozambique Channel and east of Madagascar are related to the arrival of westward propagating subtropical Rossby waves in response to the Indian Ocean dipole events. Backeberg et al. (2012) found that the mesoscale variability in the Mozambique Channel and south of Madagascar has intensified from 1993 to 2009, resulting from an increased South Equatorial Current driven by enhanced trade winds over the tropical Indian Ocean. Beal and Elipot (2016) suggested that the Agulhas Current has not intensified but broadened as a result of more eddy activity since the early 1990s based on observations.

Despite having the highest level of eddy variability in the South Indian Ocean, the interannual EKE modulations in the ARC region remain poorly explored and understood. In this study, we analyze the interannual variability of EKE around the ARC region on the basis of satellite altimetry data and high-resolution model output data. Our first objective is to describe the interannual modulations of EKE in the ARC region. The second objective is to clarify the dynamic mechanisms responsible for the detected interannual modulations.

2. ECCO2 State Estimate and Its Verification

We use the model output from the Estimating the Circulation and Climate of the Ocean, phase II (ECCO2) from 1993 to 2016. ECCO2 state estimate is based on the Massachusetts Institute of Technology general

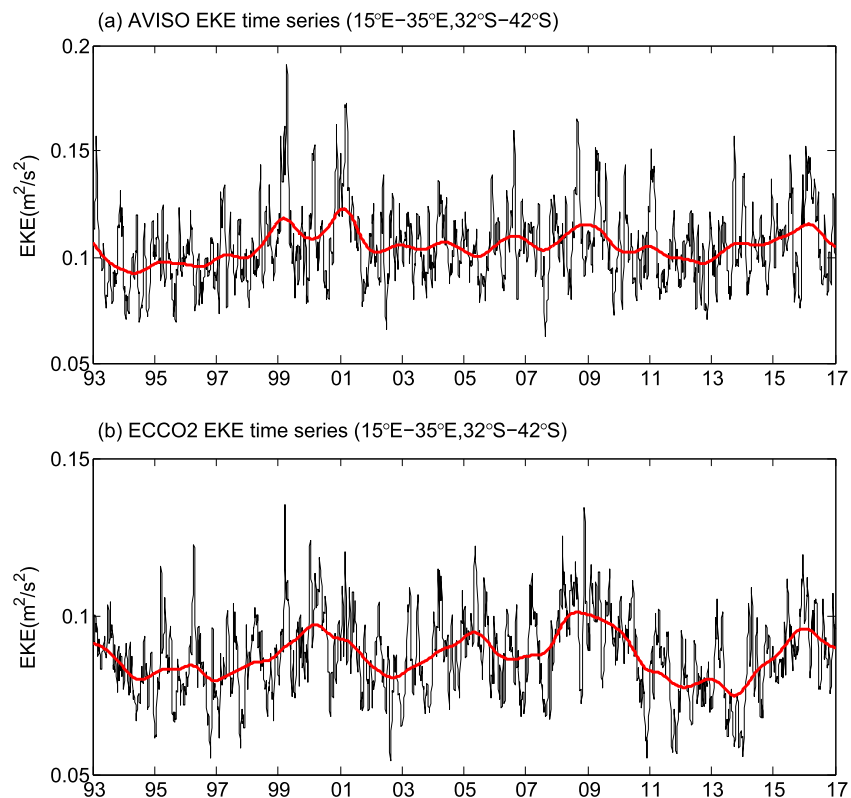


Figure 3. Time series of surface EKE in the Agulhas Return Current region of 15–35°E and 32–42°S calculated from (a) AVISO and (b) ECCO2 data. The Agulhas Return Current region is denoted by the black box in Figure 2. Black lines denote the original 3-day time series, and red lines denote the low-pass filtered time series after removal of signals shorter than annual period. AVISO = Archiving, Validation, and Interpolation of Satellite Oceanographic; ECCO2 = Estimating the Circulation and Climate of the Ocean, Phase II; EKE = eddy kinetic energy.

circulation model (Marshall et al., 1997), which is a three-dimensional global ocean model subject to hydrostatic and Boussinesq approximations. This eddy-permitting model has a mean horizontal resolution of 18 km with use of the cube sphere grid projection (cube92 version). Vertically, it has 50 levels with thicknesses varying from 10 m near the surface to 456 m near the bottom at a maximum depth of 6,150 m. The ECCO2 state estimate is a forward run using optimized control parameters, including the initial conditions, surface forcing, background vertical viscosity, and bottom drag coefficient, calculated based on the Green's function approach (Menemenlis et al., 2005). Since no observation data are inserted during the forward integration, the ECCO2 state estimate is considered to be dynamically and thermodynamically consistent (Wunsch et al., 2009). The ECCO2 state estimate has been extensively used in the past to explore the mesoscale eddy variabilities and ocean eddy energetics in different parts of the global ocean (e.g., R. Chen, Flierl, et al., 2014; Z. Chen, Wu, et al., 2014; Fu, 2009; Qiu et al., 2017; Yang et al., 2017; Zemskova et al., 2015). We use the ECCO2's 3-day-averaged data set from 1993 to 2016 in this study.

To verify the degrees of fidelity of the ECCO2 data in the region of our interest, the merged SSH anomaly data distributed by Archiving, Validation, and Interpolation of Satellite Oceanographic data (AVISO; <http://www.aviso.oceanobs.com/>) that combines simultaneous measurements from two satellite altimeters (TOPEX/Poseidon or Jason-1 and ERS or Envisat) are used in this study. The AVISO data set has a $0.25^\circ \times 0.25^\circ$ spatial resolution and a daily temporal resolution and covers the period from January 1993 to December 2016.

Mesoscale eddy variability is controlled by the basin-scale oceanic conditions. As such, before exploring the dynamical processes governing the interannual modulations of the mesoscale eddy variability, it is

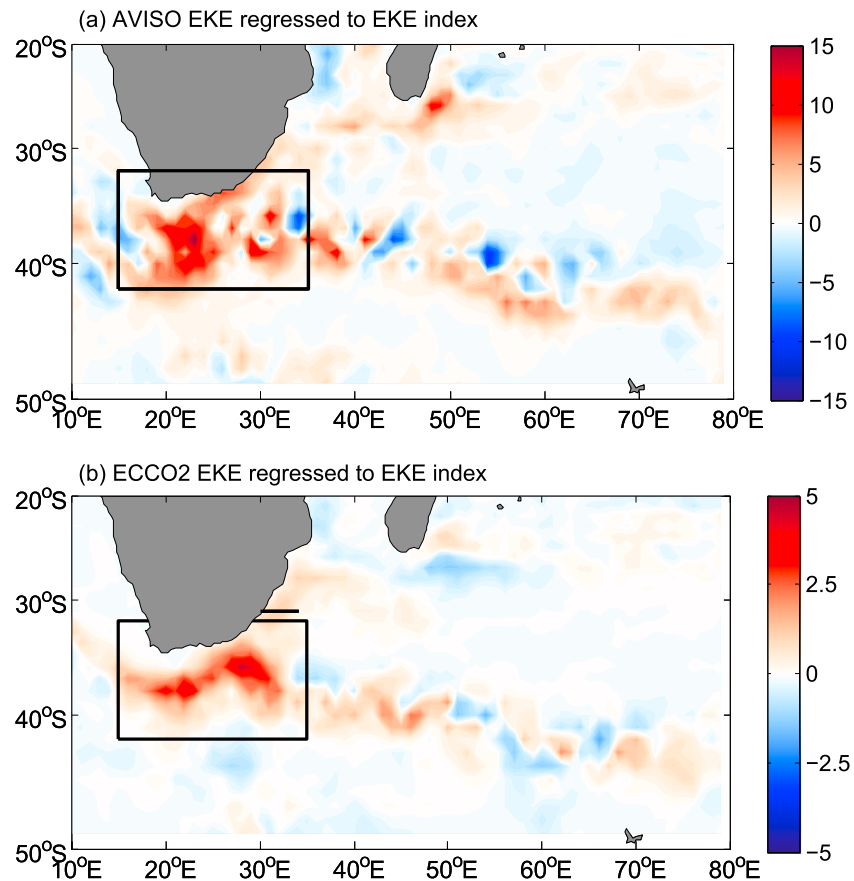


Figure 4. Spatial EKE distribution regressed to the Agulhas Return Current surface EKE index from (a) AVISO and (b) ECCO2 data. The Agulhas Return Current surface EKE index is shown by the red line in Figure 3b. AVISO = Archiving, Validation, and Interpolation of Satellite Oceanographic; ECCO2 = Estimating the Circulation and Climate of the Ocean, Phase II; EKE = eddy kinetic energy.

desirable to verify the basin-scale oceanic circulation in the Agulhas Current system in the ECCO2 state estimate based on the available satellite altimetry measurements. Figure 1 compares the time-mean SSH and surface geostrophic speed field calculated from the AVISO versus ECCO2 data surrounding the Agulhas Current system regions during the 1993–2016 period. Overall, the mean oceanic circulation estimated from ECCO2 bears close resemblance to that based on the AVISO data. The SSH patterns between Figures 1a and 1b have a linear spatial correlation $r = 0.97$, and the linear spatial correlation between the geostrophic speed patterns also reaches a high value of $r = 0.84$. In both Figures 1a and 1b, the eastward-following ARC can be readily identified by the sharp SSH gradient aligned approximately along 38°S, with its maximum geostrophic speed appears over the longitude band of 20°E to 40°E. The position of the Agulhas Plateau is located at 27°E and 39°S, and the ARC meander downstream of the Agulhas Plateau derived by the ECCO2 state estimate coincides well with the AVISO result.

3. Eddy Variability in the ARC Region

It is known that the oceanic variability is dominated by mesoscale eddy signals with temporal scales of 50–200 days (e.g., Chelton et al., 2011). To better focus on the mesoscale variability in this study, we apply a 200-day high-pass filter to the observed and modeled SSH anomaly data in order to isolate the mesoscale eddy signals. To detect the mesoscale eddy variability, we calculate the level of EKE defined by

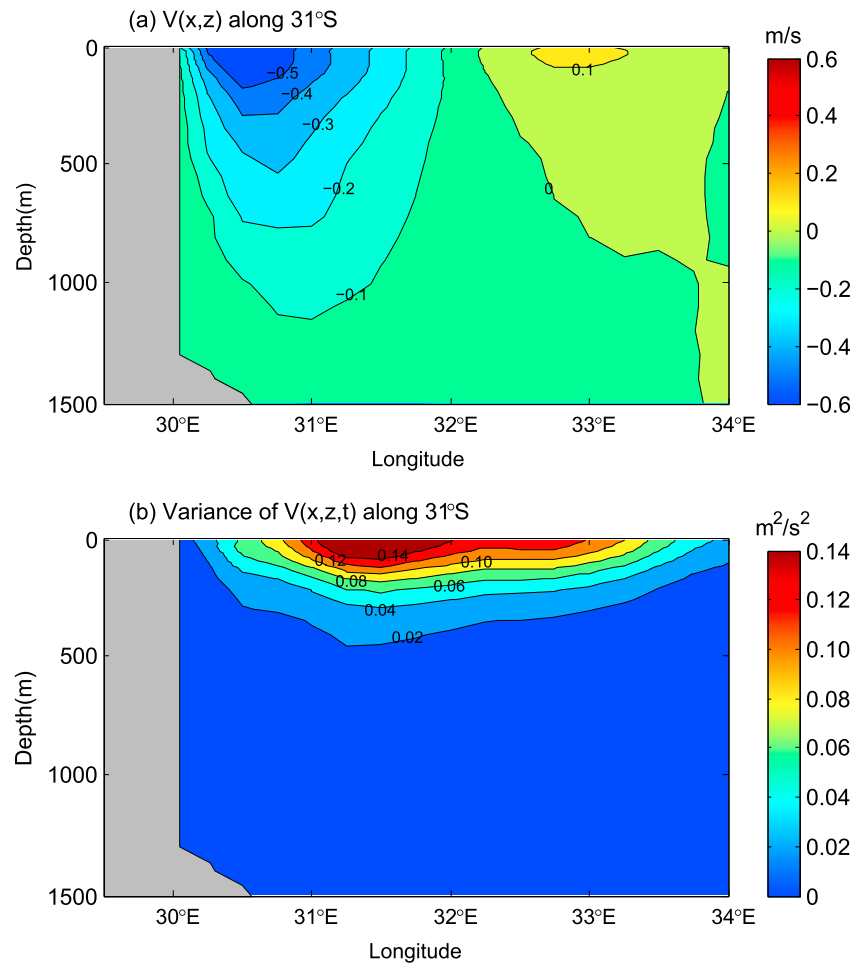


Figure 5. Longitude-depth section of Estimating the Circulation and Climate of the Ocean, Phase II (a) time-mean meridional velocity and (b) variance of meridional velocity along 31°S east of South Africa. The section location is shown by the solid line in Figure 4b.

$$\text{EKE} = \frac{g^2}{2f^2} \left[\left(\frac{\partial h'}{\partial x} \right)^2 + \left(\frac{\partial h'}{\partial y} \right)^2 \right] \quad (1)$$

where f is the Coriolis parameter, g is gravity constant, and h' is the 200-day high-pass filtered SSH anomaly data.

Figure 2 compares the spatial distribution of time-mean surface EKE level derived from the AVISO and ECCO2 data. The maximum EKE band, with an EKE level above $0.2 \text{ m}^2/\text{s}^2$, associated with the Agulhas retroflection from ECCO2 agrees relatively well with that observed by the satellite altimeters, although there is a bias for the modeled EKE peak to appear to the east when compared to the AVISO map. The linear spatial correlation between Figures 2a and 2b reaches $r = 0.78$. Aside from the Agulhas retroflection region, other areas like along the ARC path, the Agulhas Current following the east coast of South Africa, and south of Madagascar also reveal good correspondence between the modeled and observed EKE levels. In our following analyses, we will focus on the time-varying EKE signals inside the black box region of $15\text{--}35^\circ\text{E}$ and $32\text{--}42^\circ\text{S}$ in Figure 2 where the EKE level is locally maximum.

Figure 3 compares the surface EKE time series averaged in the box of $15\text{--}35^\circ\text{E}$ and $32\text{--}42^\circ\text{S}$ of our interest from the AVISO versus ECCO2 data. The black lines indicate the original 3-day time series, and the thick red lines denote the low-pass filtered EKE time series after removal of signals shorter than the annual period. In the following, we will refer the red line time series in Figure 3b as the ARC EKE

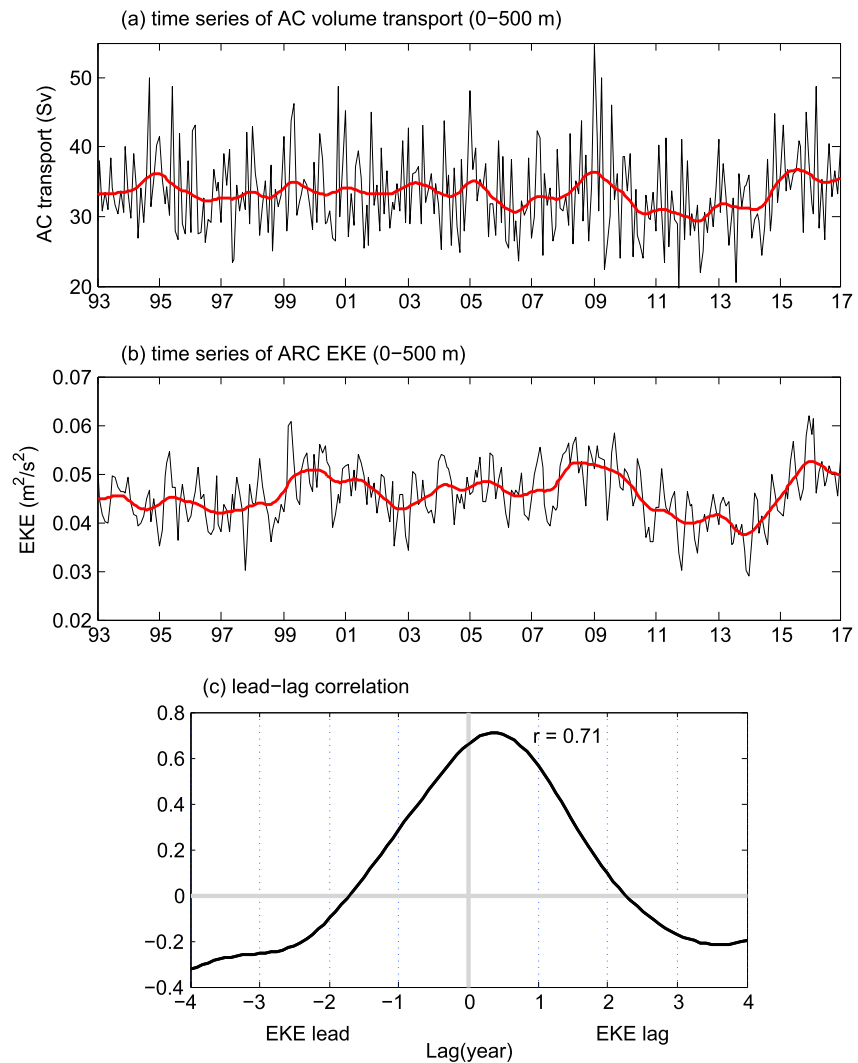


Figure 6. Monthly time series of (a) the Southward AC volume transport in the upper 500 m across 31° between 30°E to 34°E and (b) EKE in the upper 500 m in the ARC region of 15–35°E and 32–42°S. The ARC region is denoted by the black box in Figure 2b. Black lines denote the monthly averaged time series, and red line denote the low-pass filtered time series after removal of signals shorter than annual period. (c) Lagged correlation between the low-pass filtered volume transport (red line in Figure 6a) and the ARC 0–500-m EKE index (red line in Figure 6b). AC = Agulhas Current; ARC = Agulhas Return Current; EKE = eddy kinetic energy.

index, and its variability will be the target of our subsequent analyses. The time-mean EKE level based on ECCO2 in Figure 3b is 0.09 m²/s², which is 20% smaller than the value derived from AVISO in Figure 3a. One possible reason for this lower value is that the model grid resolution for ECCO2 is 0.25° × 0.25°, which is eddy-permitting and can possibly underestimate the real-ocean eddy variability. Another possible reason is that the time-mean flow strength in the ECCO2 product is biased low by about 20%; the maximum geostrophic flow speed is 0.5 m/s in ECCO2, whereas it is 0.6 m/s in the AVISO product. The ECCO2 modeled low-frequency EKE modulations, on the other hand, agree well with the AVISO signals: the linear correlation coefficient between the two low-pass filtered time series in Figure 3 reaches $r = 0.64$ and is significant at the 95% significance level (assuming the degree of freedom of the time series based on their decorrelation scales).

In order to clarify the connection between the low-frequency EKE variability in the ARC region and those in other areas, a regression analysis is conducted between the ARC EKE index and the EKE time series in the South Indian Ocean based on both the AVISO and ECCO2 data (Figure 4). The regressed spatial variability

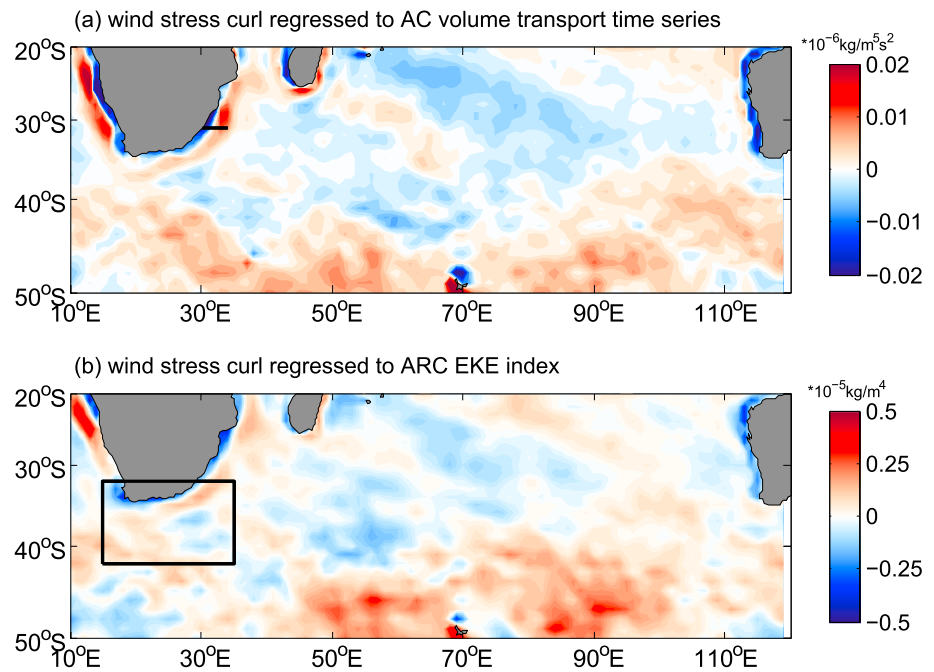


Figure 7. Wind stress curl distribution regressed to the low-pass filtered (a) AC volume transport time series and (b) ARC 0–500-m EKE index in the upper 500 m. The time series of AC volume transport and ARC 0–500-m EKE index is shown in Figures 6a and 6b, respectively. AC = Agulhas Current; ARC = Agulhas Return Current; EKE = eddy kinetic energy.

from the ECCO2 state estimate is overall consistent with that from the AVISO data: high variability can be seen in the Agulhas retroflexion region, along the downstream path of ARC, as well as in the upstream Agulhas Current region east of South Africa. From the above analyses, it is clear that the ECCO2 state estimate is capable of simulating the observed EKE signals both in terms of their spatial patterns (Figures 2 and 4) and of their interannual modulations (Figure 3).

4. The Agulhas Current Inflow Transport

It is of interest to note from Figure 4 that the interannual EKE modulations in the ARC region seem to be connected to the upstream Agulhas Current variability. To clarify this connection further, we first evaluate the volume transport in the Agulhas Current region using the ECCO2 output. Figure 5a shows the longitude-depth section of the time-mean meridional velocity (positive northward) along 31°S. As shown by the black line in Figure 4b, this section along 31°S traverses the Agulhas Current just to the north of the ARC EKE index box of our interest. The time-mean Agulhas Current across this section has a southward surface-intensified velocity core at about 0.6 m/s and extends to the 1,000-m depth where the meridional velocity becomes 0.1 m/s within the longitudinal width from 30°E to 32°E. The corresponding variance of meridional velocity across this section is largely confined to the upper 500-m layer from the African continent to 34°E as shown in Figure 5b. By integrating the meridional velocity from the South African coast at 30°E to 34°E, we evaluate the volume transport of the Agulhas Current across 31°S in the upper 500-m depth. Notice that the northward flow is ignored when we calculate the cumulative Agulhas Current volume transport. As shown in Figure 6a, the Agulhas Current volume transport varies generally from 20 to 50 Sv with strong decadal fluctuations. For comparison, we plot in Figure 6b the ECCO2 EKE time series averaged in the upper 500-m layer in the same ARC region of 15–35°E and 32–42°S as that introduced in section 3. The black line denotes the monthly time series, and the red line denotes the low-pass filtered time series after removal of signals shorter than the annual period. To explore the effect by the time-varying Agulhas Current volume transport, we compute the lagged correlations between its low-pass filtered time series (the red line in Figure 6a) and the EKE interannual modulations (the red line in Figure 6b). As shown in Figure 6c, the maximum correlation reaches as high as $r = 0.71$ (significant at the 95% significance level) when the Agulhas Current volume transport leads the downstream EKE in the ARC region by about 4 months. Notice that this lagged correlation result is

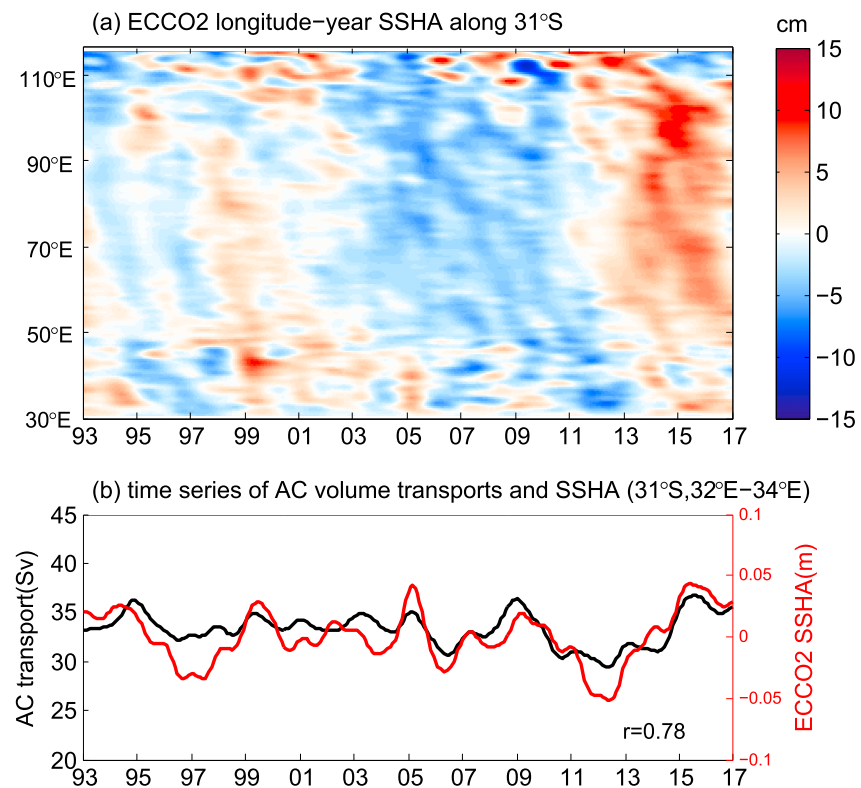


Figure 8. (a) Time-longitude plot of the low-pass filtered SSH anomalies along 31°S across the South Indian Ocean basin. (b) Monthly time series of the low-pass filtered AC volume transport (black line; same as the red line in Figure 6a) and SSH anomalies (red line) along 31°S between 32°E and 34°E. SSHA = sea surface height anomaly; ECCO2 = Estimating the Circulation and Climate of the Ocean, Phase II; AC = Agulhas Current.

similarly valid when we choose different zonal transects between 30°S and 34°S. In the following section, we will focus on the mechanism responsible for the interannual volume transport changes in the upstream Agulhas Current.

5. Mechanism Responsible for Interannual EKE Modulation

Given that the Agulhas Current constitutes the compensating western boundary current for the wind-driven subtropical gyre in the subtropical Indian Ocean, it is natural to hypothesize that its interannual volume transport modulations are caused by changes in the basin-wide surface wind stress curl forcing. To test this hypothesis, we examine the wind stress data of the ERA-Interim atmospheric reanalysis (http://data-portal.ecmwf.int/data/d/interim_daily/) produced by the European Centre for Medium-Range Weather Forecasts (Dee et al., 2011). The ERA-Interim data to be analyzed in our study cover the same period as the ECCO2 state estimate; it has a spatial resolution of $0.75^\circ \times 0.75^\circ$ and a monthly temporal resolution and has been analyzed extensively in previous studies (e.g., England et al., 2014; Holland & Kwok, 2012).

A regression analysis between the low-pass filtered Agulhas Current volume transport time series (Figure 6a, red line) and the wind stress curl time series in the Southern Indian Ocean reveals that the regressed wind stress curl east of the Agulhas Current appears mostly negative, which is consistent with the spin-up of the wind-driven subtropical gyre and southward-flowing Agulhas Current through enhanced Ekman pumping (Figure 7a). In comparison, the regression analysis between the low-pass filtered EKE time series in the ARC region (Figure 6b, red line) and the wind stress curl time series is shown in Figure 7b. The regressed spatial pattern bears a good resemblance to Figure 7a, indicating that the basin-scale wind forcing has a similar influence on the downstream EKE signals in the ARC region.

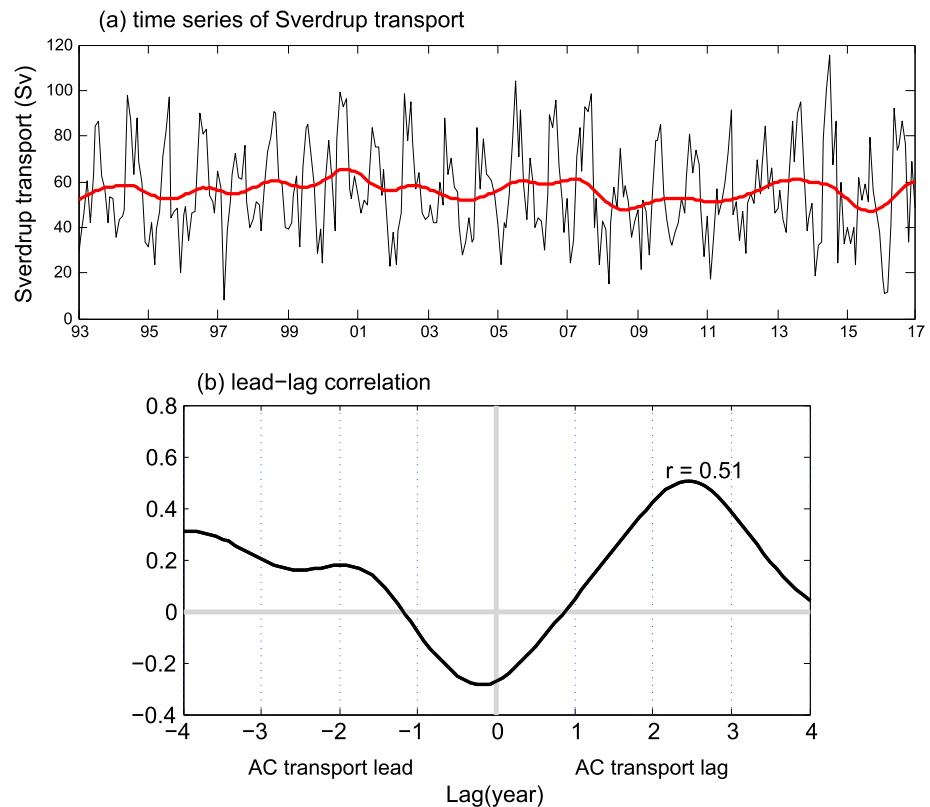


Figure 9. (a) Monthly time series of Sverdrup transport from the eastern boundary to 34°E along 31°S. Black line denotes the monthly averaged time series, and red line denotes the low-pass filtered time series after removal of signals shorter than annual period. (b) Lagged correlation between the low-pass filtered AC volume transport (red line in Figure 6a) and the Sverdrup transport (red line in Figure 9a). AC = Agulhas Current.

Physically, the wind stress forcing in the Indian Ocean Subtropical gyre generates positive SSH anomalies through Ekman pumping by wind stress curl anomalies. These wind-induced SSH anomaly signals propagate to the west as baroclinic Rossby waves and change the Agulhas Current transport through SSH gradient according to geostrophy.

Figure 8a shows the time-longitude plot of SSH anomalies along 31°S, the latitude we chose to calculate the Agulhas Current volume transport (Figure 6a). It is clear that the SSH anomaly signals associated with the wind forcing propagate westward from the eastern boundary around 116°E at the baroclinic Rossby wave speed of 0.05 m/s across the South Indian Ocean basin (Chelton et al., 2011) and extend close to the western boundary. Figure 8b compares the low-pass filtered time series of the Agulhas Current volume transport (same as the red line in Figure 6a) and the SSH anomalies averaged between 32°E and 34°E along 31°S east of the Agulhas Current. The two time series match favorably with the linear correlation coefficient reaching $r = 0.78$ (significant at the 95% significance level), indicating the coming SSH anomaly signals determine the low-frequency variability of the Agulhas Current upstream of the ARC region.

To further quantify the relationship between the Agulhas Current transport and the wind stress forcing, we calculate the Sverdrup transport driven by the wind stress curl from the eastern boundary to 34°E along 31°S (Figure 9a) and compute the lagged correlation between the low-pass filtered Agulhas Current transport (the red line in Figure 6a) and the Sverdrup transport (the red line in Figure 9a). As shown in Figure 9b, the maximum correlation between the Agulhas Current transport and the Sverdrup transport reaches a maximum of $r = 0.51$ (significant at the 95% significance level) when the Agulhas Current transport lags the Sverdrup transport by about 2.5 years. This 2.5-year lag is consistent with the time it takes for baroclinic Rossby waves to cross from the center of the South Indian Ocean basin (or the center of the wind stress curl forcing) near 74°E to the Agulhas Current longitude of 34°E along 31°S. The above comparison result confirms

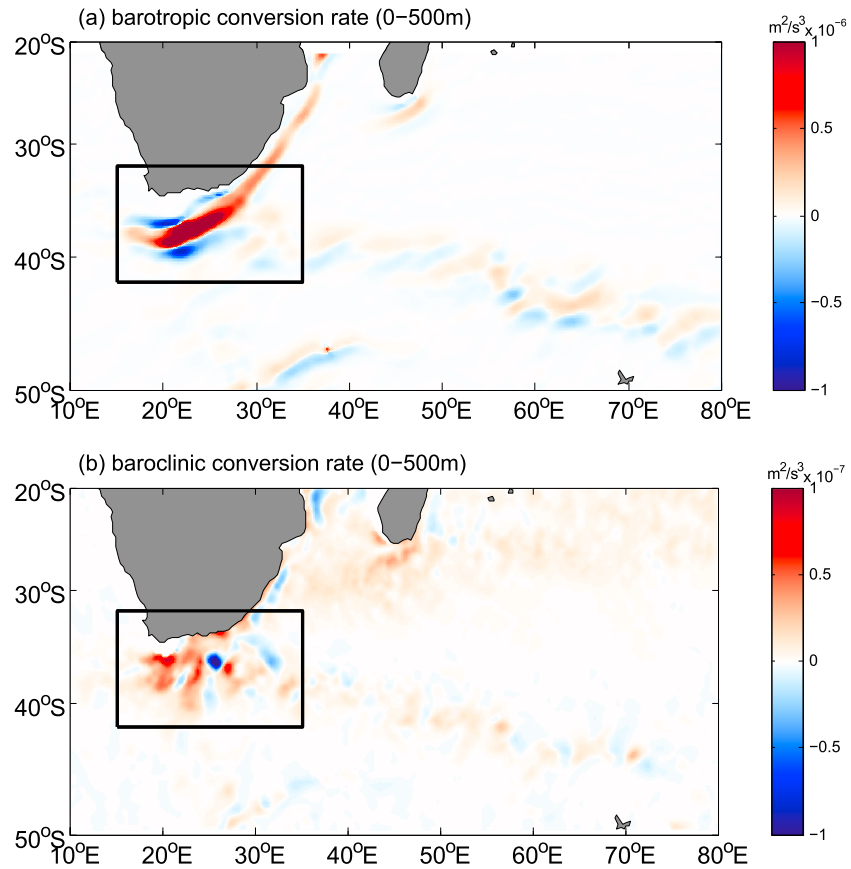


Figure 10. Spatial distributions of time mean (a) barotropic conversion rate and (b) baroclinic conversion rate in the upper 500 m. Notice that the color bar scales are different.

that the interannual Agulhas current transport variability is mainly driven by the basin-wide surface wind stress curl forcing.

To connect the upstream Agulhas Current variability to the interannual EKE modulations in the ARC region, we examine the barotropic and baroclinic eddy energy conversion rate in the upper 500-m layer of the ARC region. Here the two conversion rates are defined as follows:

$$\text{barotropic conversion rate} = - \left(\overline{u'u'} \frac{\partial \bar{u}}{\partial x} + \overline{u'v'} \left(\frac{\partial \bar{v}}{\partial x} + \frac{\partial \bar{u}}{\partial y} \right) + \overline{v'v'} \frac{\partial \bar{v}}{\partial y} \right) \quad (2)$$

and

$$\text{baroclinic conversion rate} = g \frac{\overline{u'\rho'} \frac{\partial \bar{\rho}}{\partial x} + \overline{v'\rho'} \frac{\partial \bar{\rho}}{\partial y}}{d\bar{\rho}/dz} \quad (3)$$

where u' and v' denote the 200-day high-pass filtered horizontal velocity anomalies representing the mesoscale eddy signals, and \bar{u} and \bar{v} are the background horizontal currents with time scales longer than 200 days. Similarly, ρ' denotes the 200-day high-pass filtered potential density, and $\bar{\rho}$ is the background potential density with time scale longer than 200 days. In (3), $\bar{\rho}(z)$ represents the domain-averaged referenced potential density, and g is the gravity constant. Physically, equation (2) represents the conversion from mean kinetic energy to EKE through turbulent Reynolds stresses, and a positive value is indicative of barotropic instability in the slowly varying background flow system. Equation (3), on the other hand, represents the conversion from mean potential energy to eddy potential energy, and a positive value indicates the occurrence of baroclinic instability by the background mean circulation.

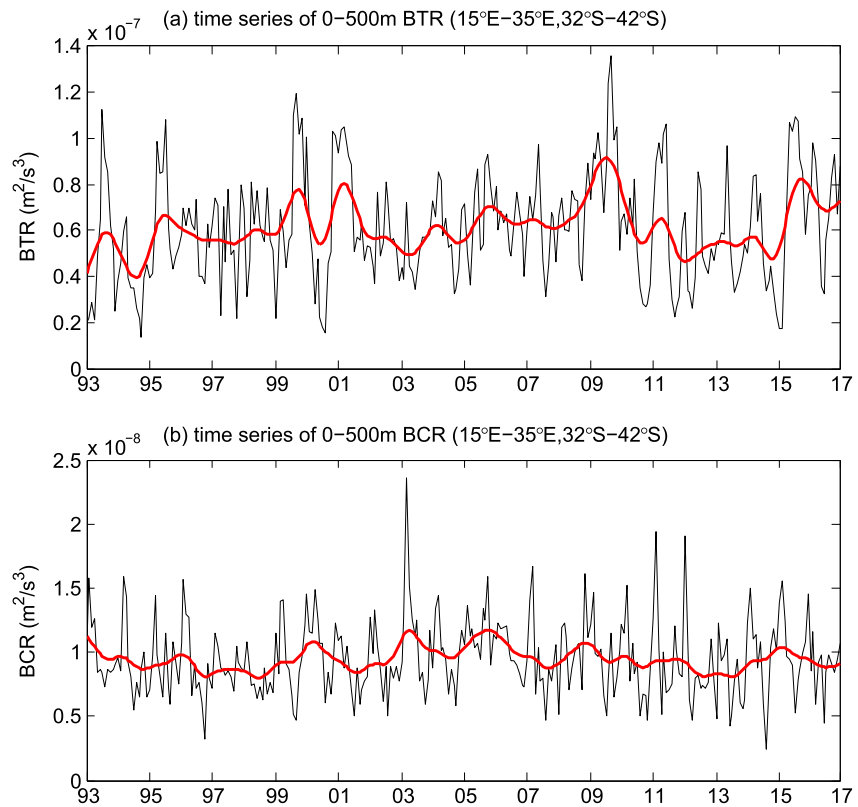


Figure 11. Monthly time series of (a) barotropic conversion rate and (b) baroclinic conversion rate in the upper 500 m in the region of 15–35°E, 32–42°S (see the box in Figure 10). Black lines denote the monthly averaged time series, and red line denote the low-pass filtered time series after removal of signals shorter than annual period. BTR = barotropic conversion rate; BCR = baroclinic conversion rate.

The spatial distribution of the barotropic and baroclinic conversion rates averaged in the upper 500 m are shown in Figure 10. The barotropic conversion rate (Figure 10a) exhibits consistent positive values along the path of the Agulhas Current and reaches a regionally maximum level in the ARC region, especially in the retroflexion area. This result is consistent with the previous theoretical and numerical studies that identified the importance of barotropic instability in the Agulhas Current region (de Ruijter, Van Leeuwen, et al., 1999; Elipot & Beal, 2015; Tsugawa & Hasumi, 2010). In contrast, the baroclinic conversion rate (Figure 10b) appears less positive in the ARC region and with a level nearly an order of magnitude smaller than the barotropic conversion rate. By comparing Figures 9a and 9b, we can see that the major energy source for EKE in the ARC region is via the barotropic instability pathway, and this energy transfer process occurs most prominently in the retroflexion area off the southern tip of Africa.

Finally, it is of interest to quantify the contributions by barotropic and baroclinic instability to the observed EKE modulations. To do so, we focus on the ARC region of 15–35°E and 32–42°S (the black box in Figure 10), the same region as selected in Figure 2. Figure 11 compares the time series of barotropic and baroclinic conversion rates averaged in this focus are; the black lines denote the monthly averaged time series and the red lines the low-pass filtered time series. On the interannual time scales, the barotropic conversion rate (Figure 11a) and the ARC EKE modulations (Figure 6b) are reasonably well correlated with the linear correlation coefficient reaching $r = 0.74$. In contrast, the linear correlation coefficient between baroclinic conversion rate (Figure 11b) and the ARC EKE modulations (Figure 6b) is low, at $r = 0.31$ only. Dynamically, this confirms that as the upstream Agulhas Current volume transport changes in response to the basin-scale wind forcing, the strength of the background circulation in the Agulhas retroflexion region fluctuates, resulting in modulations in the intensity of the regional barotropic instability associated with the horizontal shear of the background circulation. It is this temporally modulating barotropic instability that is responsible for the interannual EKE modulations in the ARC region.

6. Summary

The interannual EKE modulations in the ARC region are investigated in this study on the basis of the satellite altimeter observations and the ECCO2 state estimate for the period of 1993–2016. The regional EKE level reaches a maximum off the southern tip of Africa in 15–35°E and 32–42°S (Figure 2). The EKE signal in this region undergoes pronounced interannual modulations (Figure 3), and clarifying the dynamics responsible for the observed interannual variability forms the main focus of our analyses. Being part of the western boundary current outflow in the wind-driven subtropical gyre, the interannual EKE modulations in the ARC region are externally induced by the time-varying wind stress forcing across the South Indian Ocean subtropical basin. Specifically, the time-varying wind stress curl generates SSH anomalies through anomalous Ekman pumping/suction in the Subtropical Indian Ocean, and these wind-induced SSH anomaly signals propagate to the west as baroclinic Rossby waves. Upon approaching the western boundary off South Africa, these SSH anomalies alter the Agulhas Current volume transport through geostrophic SSH difference (Figure 8). After a delay of approximately 4 months, changes in the inflow Agulhas Current volume transport are found to modify the intensity of barotropic instability in the downstream ARC region and force the interannual EKE modulations there (Figures 6 and 10). In particular, the region around the Agulhas retroflexion is where the EKE transfer from the mean flow to eddies, or barotropic instability, takes place most prominently (Figure 11). Although we have in this study clarified the mechanism responsible for the interannual eddy variability in the ARC region, future studies are needed to explore how this eddy variability and its interannual modulations could impact on the water mass property and air-sea interaction changes such as in the Agulhas leakages and in the downstream ARC region east of 35°E.

Acknowledgments

We thank the two reviewers for their detailed and constructive comments that helped improve an early version of the paper. The ECCO2 state estimate data set is available at http://apdr.csoest.hawaii.edu/datadoc/ecco2_cube92.php, the AVISO SSH data at <http://www.aviso.oceanobs.com/>, and the ERA-Interim wind stress data at http://data-portal.ecmwf.int/data/d/interim_daily/. Xiaopei Lin is supported by the China's National Key Research and Development Projects (2016YFA0601803), the National Natural Science Foundation of China (41490641, 41521091, and U1606402), and the Qingdao National Laboratory for Marine Science and Technology (2017ASKJ01). Yanan Zhu acknowledges support from the China Scholarship Council.

References

- Arhan, M., Mercier, H., & Park, Y. H. (2003). On the deep water circulation of the eastern South Atlantic Ocean. *Deep Sea Research Part I: Oceanographic Research Papers*, 50(7), 889–916. [https://doi.org/10.1016/S0967-0637\(03\)00072-4](https://doi.org/10.1016/S0967-0637(03)00072-4)
- Arruda, W., Zharkov, V., Deremble, B., Nof, D., & Chassignet, E. (2014). A new model of current retroflexion applied to the westward protrusion of the Agulhas current. *Journal of Physical Oceanography*, 44(12), 3118–3138. <https://doi.org/10.1175/JPO-D-14-0054.1>
- Backeberg, B. C., Penven, P., & Rouault, M. (2012). Impact of intensified Indian Ocean winds on mesoscale variability in the Agulhas system. *Nature Climate Change*, 2(8), 608–612. <https://doi.org/10.1038/nclimate1587>
- Beal, L. M., Chereskin, T. K., Lenn, Y. D., & Elipot, S. (2006). The sources and mixing characteristics of the Agulhas Current. *Journal of Physical Oceanography*, 36(11), 2060–2074. <https://doi.org/10.1175/JPO2964.1>
- Beal, L. M., De Ruijter, W. P., Biastoch, A., Zahn, R., & Cronin, R. (2011). On the role of the Agulhas system in ocean circulation and climate. *Nature*, 472(7344), 429–436. <https://doi.org/10.1038/nature09983>
- Beal, L. M., & Elipot, S. (2016). Broadening not strengthening of the Agulhas Current since the early 1990s. *Nature*, 540(7634), 570–573. <https://doi.org/10.1038/nature19853>
- Belkin, I. M., & Gordon, A. L. (1996). Southern Ocean fronts from the Greenwich meridian to Tasmania. *Journal of Geophysical Research*, 101(C2), 3675–3696. <https://doi.org/10.1029/95JC02750>
- Biastoch, A., Böning, C. W., & Lutjeharms, J. R. E. (2008). Agulhas leakage dynamics affects decadal variability in Atlantic overturning circulation. *Nature*, 456(7221), 489–492. <https://doi.org/10.1038/nature07426>
- Biastoch, A., Böning, C. W., Schwarzkopf, F. U., & Lutjeharms, J. R. (2009). Increase in Agulhas leakage due to poleward shift of Southern Hemisphere westerlies. *Nature*, 462(7272), 495–498. <https://doi.org/10.1038/nature08519>
- Boebel, O., Lutjeharms, J., Schmid, C., Zenk, W., Rossby, T., & Barron, C. (2003). The cape cauldron: A regime of turbulent inter-ocean exchange. *Deep Sea Research Part II Topical Studies in Oceanography*, 50(1), 57–86. [https://doi.org/10.1016/S0967-0645\(02\)00379-X](https://doi.org/10.1016/S0967-0645(02)00379-X)
- Chassignet, E. P., & Boudra, D. B. (1988). Dynamics of Agulhas retroflexion and ring formation in a numerical model. Part II. Energetics and ring formation. *Journal of Physical Oceanography*, 18(2), 304–319. [https://doi.org/10.1175/1520-0485\(1988\)018<0304:DOARAR>2.0.CO;2](https://doi.org/10.1175/1520-0485(1988)018<0304:DOARAR>2.0.CO;2)
- Chelton, D. B., Schlax, M. G., & Samelson, R. M. (2011). Global observations of nonlinear mesoscale eddies. *Progress in Oceanography*, 91(2), 167–216. <https://doi.org/10.1016/j.pocean.2011.01.002>
- Chen, R., Flierl, G. R., & Wunsch, C. (2014). A description of local and nonlocal eddy-mean flow interaction in a global eddy-permitting state estimate. *Journal of Physical Oceanography*, 44(9), 2336–2352. <https://doi.org/10.1175/JPO-D-14-0009.1>
- Chen, Z., Wu, L., Qiu, B., Sun, S., & Jia, F. (2014). Seasonal variation of the South Equatorial Current bifurcation off Madagascar. *Journal of Physical Oceanography*, 44(2), 618–631. <https://doi.org/10.1175/JPO-D-13-0147.1>
- de Ruijter, W. P., Biastoch, A., Drijfhout, S. S., Lutjeharms, J. R., Matano, R. P., Pichevin, T., & Weijer, W. (1999). Indian-Atlantic interocean exchange: Dynamics, estimation and impact. *Journal of Geophysical Research*, 104(C9), 20885–20910. <https://doi.org/10.1029/1998JC900099>
- de Ruijter, W. P., van Aken, H. M., Beier, E. J., Lutjeharms, J. R., Matano, R. P., & Schouten, M. W. (2004). Eddies and dipoles around South Madagascar: Formation, pathways and large-scale impact. *Deep Sea Research Part I: Oceanographic Research Papers*, 51(3), 383–400. <https://doi.org/10.1016/j.dsr.2003.10.011>
- de Ruijter, W. P., Van Leeuwen, P. J., & Lutjeharms, J. R. (1999). Generation and evolution of Natal Pulses: Solitary meanders in the Agulhas Current. *Journal of Physical Oceanography*, 29(12), 3043–3055. [https://doi.org/10.1175/1520-0485\(1999\)029<3043:GAEONP>2.0.CO;2](https://doi.org/10.1175/1520-0485(1999)029<3043:GAEONP>2.0.CO;2)
- Dee, D. P., Uppala, S. M., Simmons, A. J., Berrisford, P., Poli, P., Kobayashi, S., et al. (2011). The ERA-interim reanalysis: Configuration and performance of the data assimilation system. *Quarterly Journal of the Royal Meteorological Society*, 137(656), 553–597. <https://doi.org/10.1002/qj.828>
- Dencausse, G., Arhan, M., & Speich, S. (2010). Spatio-temporal characteristics of the Agulhas Current retroflexion. *Deep Sea Research Part I: Oceanographic Research Papers*, 57(11), 1392–1405. <https://doi.org/10.1016/j.dsr.2010.07.004>

- Dijkstra, H. A., & de Ruijter, W. P. (2001). Barotropic instabilities of the Agulhas Current system and their relation to ring formation. *Journal of Marine Research*, 59(4), 517–533. <https://doi.org/10.1357/002224001762842172>
- Elipot, S., & Beal, L. M. (2015). Characteristics, energetics, and origins of Agulhas Current meanders and their limited influence on ring shedding. *Journal of Physical Oceanography*, 45(9), 2294–2314. <https://doi.org/10.1175/JPO-D-14-0254.1>
- Elipot, S., & Beal, L. M. (2018). Observed Agulhas Current sensitivity to interannual and long-term trend atmospheric forcings. *Journal of Climate*, 31(8), 3077–3098.
- England, M. H., McGregor, S., Spence, P., Meehl, G. A., Timmermann, A., Cai, W., et al. (2014). Recent intensification of wind-driven circulation in the Pacific and the ongoing warming hiatus. *Nature Climate Change*, 4(3), 222–227. <https://doi.org/10.1038/nclimate2106>
- Fu, L. L. (2009). Pattern and velocity of propagation of the global ocean eddy variability. *Journal of Geophysical Research*, 114, C11017. <https://doi.org/10.1029/2009JC005349>
- Gordon, A. L. (2003). The brawnierest retroflection. *Nature*, 421(6926), 904–905. <https://doi.org/10.1038/421904a>
- Gordon, A. L., Weiss, R. F., Smethie, W. M., & Warner, M. J. (1992). Thermocline and intermediate water communication between the south Atlantic and Indian oceans. *Journal of Geophysical Research*, 97(C5), 7223–7240.
- Holland, P. R., & Kwok, R. (2012). Wind-driven trends in Antarctic sea-ice drift. *Nature Geoscience*, 5(12), 872–875. <https://doi.org/10.1038/ngeo1627>
- Jia, F., Wu, L., Lan, J., & Qiu, B. (2011). Interannual modulation of eddy kinetic energy in the southeast Indian Ocean by southern annular mode. *Journal of Geophysical Research*, 116, C02029. <https://doi.org/10.1029/2010JC006699>
- Leber, G. M., Beal, L. M., & Elipot, S. (2017). Wind and current forcing combine to drive strong upwelling in the Agulhas current. *Journal of Physical Oceanography*, 47(1), 123–134. <https://doi.org/10.1175/JPO-D-16-0079.1>
- Lutjeharms, J. R. (2006). *The Agulhas Current* (Vol. 2). Berlin: Springer.
- Lutjeharms, J. R., & Anson, I. J. (2001). The Agulhas Return Current. *Journal of Marine Systems*, 30(1–2), 115–138. [https://doi.org/10.1016/S0924-7963\(01\)00041-0](https://doi.org/10.1016/S0924-7963(01)00041-0)
- Lutjeharms, J. R., & van Ballegooyen, R. C. (1988). The retroflection of the Agulhas Current. *Journal of Physical Oceanography*, 18(11), 1570–1583. [https://doi.org/10.1175/1520-0485\(1988\)018<1570:TROTAC>2.0.CO;2](https://doi.org/10.1175/1520-0485(1988)018<1570:TROTAC>2.0.CO;2)
- Marshall, J., Adcroft, A., Hill, C., Perelman, L., & Heisey, C. (1997). A finite-volume, incompressible Navier Stokes model for studies of the ocean on parallel computers. *Journal of Geophysical Research*, 102(C3), 5753–5766. <https://doi.org/10.1029/96JC02775>
- Menemenlis, D., Fukumori, I., & Lee, T. (2005). Using Green's functions to calibrate an ocean general circulation model. *Monthly Weather Review*, 133(5), 1224–1240. <https://doi.org/10.1175/MWR2912.1>
- Palastanga, V., Leeuwen, P. J. V., & Ruijter, W. P. M. (2006). A link between low-frequency mesoscale eddy variability around Madagascar and the large-scale Indian Ocean variability. *Journal of Geophysical Research*, 111, C09029. <https://doi.org/10.1029/2005JC003081>
- Qiu, B., & Chen, S. (2010). Interannual variability of the North Pacific Subtropical Countercurrent and its associated mesoscale eddy field. *Journal of Physical Oceanography*, 40(1), 213–225. <https://doi.org/10.1175/2009JPO4285.1>
- Qiu, B., Chen, S., & Schneider, N. (2017). Dynamical links between the decadal variability of the Oyashio and Kuroshio extensions. *Journal of Climate*, 30(23), 9591–9605. <https://doi.org/10.1175/JCLI-D-17-0397.1>
- Schouten, M. W., de Ruijter, W. P., Van Leeuwen, P. J., & Ridderinkhof, H. (2003). Eddies and variability in the Mozambique Channel. *Deep Sea Research Part II: Topical Studies in Oceanography*, 50(12–13), 1987–2003. [https://doi.org/10.1016/S0967-0645\(03\)00042-0](https://doi.org/10.1016/S0967-0645(03)00042-0)
- Song, Q., Gordon, A. L., & Visbeck, M. (2004). Spreading of the Indonesian Throughflow in the Indian Ocean. *Journal of Physical Oceanography*, 34(4), 772–792. [https://doi.org/10.1175/1520-0485\(2004\)034<0772:SOTITI>2.0.CO;2](https://doi.org/10.1175/1520-0485(2004)034<0772:SOTITI>2.0.CO;2)
- Speich, S., Lutjeharms, J. R., Penven, P., & Blanke, B. (2007). Role of bathymetry in Agulhas Current configuration and behaviour. *Geophysical Research Letters*, 33, L23611. <https://doi.org/10.1029/2006GL027157>
- Tsugawa, M., & Hasumi, H. (2010). Generation and growth mechanism of the Natal Pulse. *Journal of Physical Oceanography*, 40(7), 1597–1612. <https://doi.org/10.1175/2010JPO4347.1>
- Van Aken, H. M., Van Veldhoven, A. K., Veth, C., De Ruijter, W. P. M., Van Leeuwen, P. J., Drijfhout, S. S., et al. (2003). Observations of a young Agulhas ring, Astrid, during MARE in March 2000. *Deep Sea Research Part II: Topical Studies in Oceanography*, 50(1), 167–195. [https://doi.org/10.1016/S0967-0645\(02\)00383-1](https://doi.org/10.1016/S0967-0645(02)00383-1)
- Volkov, D. L., & Fu, L. L. (2011). Interannual variability of the Azores current strength and eddy energy in relation to atmospheric forcing. *Journal of Geophysical Research*, 116, C11011. <https://doi.org/10.1029/2011JC007271>
- Weijer, W., De Ruijter, W. P., Sterl, A., & Drijfhout, S. S. (2002). Response of the Atlantic overturning circulation to South Atlantic sources of buoyancy. *Global and Planetary Change*, 34(3–4), 293–311. [https://doi.org/10.1016/S0921-8181\(02\)00121-2](https://doi.org/10.1016/S0921-8181(02)00121-2)
- Weijer, W., Zharkov, V., Nof, D., Dijkstra, H. A., Ruijter, W. P., Scheltinga, A. T., & Wubs, F. (2013). Agulhas ring formation as a barotropic instability of the retroflection. *Geophysical Research Letters*, 40, 5435–5438. <https://doi.org/10.1002/2013GL057751>
- Wunsch, C., Heimbach, P., Ponte, R. M., & Fukumori, I. (2009). The global general circulation of the ocean estimated by the ECCO-Consortium. *Oceanography*, 22(2), 88–103. <https://doi.org/10.5670/oceanog.2009.41>
- Yang, Y., San Liang, X., Qiu, B., & Chen, S. (2017). On the decadal variability of the eddy kinetic energy in the Kuroshio extension. *Journal of Physical Oceanography*, 47(5), 1169–1187. <https://doi.org/10.1175/JPO-D-16-0201.1>
- Zemskova, V. E., White, B. L., & Scotti, A. (2015). Available potential energy and the general circulation: Partitioning wind, buoyancy forcing, and diapycnal mixing. *Journal of Physical Oceanography*, 45(6), 1510–1531. <https://doi.org/10.1175/JPO-D-14-0043.1>